

Sparse approximations in spatio-temporal point-process models

Botond Cseke¹, Andrew Zammit Mangion², Guido Sanguinetti¹ and Tom Heskes³

¹School of Informatics, University of Edinburgh

²School of Geographical Sciences, University of Bristol

³Faculty of Science, Radboud University Nijmegen

December 3, 2024

Abstract

Analysis of spatio-temporal point patterns plays an important role in several disciplines, yet inference in these systems remains computationally challenging due to the high resolution modelling generally required by large data sets and the analytically intractable likelihood function. Here, we exploit the sparsity structure of a fully-discretised log-Gaussian Cox process model by using expectation constrained approximate inference. The resulting family of expectation propagation algorithms scale well with the state dimension and the length of the temporal horizon with moderate loss in distributional accuracy. They hence provide a flexible and faster alternative to both the filtering-smoothing type algorithms and the approaches which implement the Laplace method or expectation propagation on (block) sparse latent Gaussian models. We demonstrate the use of the proposed method in the reconstruction of conflict intensity levels in Afghanistan from a WikiLeaks data set.

Keywords: latent Gaussian models, linear dynamical systems, log Gaussian Cox process, approximate inference, expectation propagation, sparse inference.

1 Introduction

Spatio-temporal point-process modelling finds application in several fields such as epidemiology, (Diggle et al., 2005), ecology (Hooten and Wikle, 2008) and criminology (Rodrigues and Diggle, 2012). However, despite their importance and prevalence, inference in these systems remains computationally challenging. Markov chain Monte Carlo (MCMC) is frequently employed, however sampling is expensive and the problems under investigation are generally only of moderate size and complexity. On the other hand deterministic approximate inference methods for inference are rapidly gaining popularity in this field. These approaches can be classified as dynamic or static: The former class consists of filtering-smoothing type approaches such as the variational approach in Zammit-Mangion et al. (2012a) or the expectation propagation (EP) algorithm exploiting low rank approximations in Hartikainen et al. (2011). The static approaches cast the discretised model as a latent (sparse) Gaussian block model and apply the Laplace method (Rue et al., 2009) or a corresponding EP algorithm (e.g. Cseke and Heskes, 2011). However, the computational scaling of these approaches is fixed and they may become untenable for large state dimensionality and long time series.

In this paper we derive an EP algorithm that reduces the computational complexity not by the above mentioned low rank approaches, but by exploiting the sparsity (in canonical/precision parameters) of the underlying latent Gaussian model. The approach we take exploits this sparsity in a similar way as in Rue et al. (2009) and Cseke and Heskes (2011), however, the crucial step is the distribution of the computation. The expensive (sparse) linear algebraic operations are performed not on the (concatenated) block model, but instead on the two-time slice marginals characteristic to the dynamic approaches. The complexity of these local computations depends on the graph structure of the expectation constraints imposed on the approximate marginals, namely the sparsity structure of the Gaussian messages that these constraints result in. We introduce a class of constraints that result in messages having the following precision structures: (i) diagonal (factored messages), (ii) spanning tree (iii) chordal and finally (iv) fully connected (full messages). The latter corresponds to the standard filtering-smoothing type EP algorithm. An algorithmically similar approach to (i) for discrete Bayesian networks is presented in Murphy and Weiss (2001). Comparisons on data generated from the model show that these algorithms scale well and depending on the complexity of the messages we can do approximate inference on hundreds or a few thousands of state variables and hundreds of time-steps with reasonable time and memory requirements.

This paper is structured as follows. In Section 2 we introduce the log-Gaussian Cox process and present the discretisation and approximation steps that simplify this model to a dynamic latent Gaussian model with non-Gaussian observations. In Section 3 we derive a class of dynamic EP algorithms that exploit sparse interaction structures. In Section 4 we discuss the performance of these algorithms and apply them to the WikiLeaks Afghan War Diary, a data set containing tens of thousands of events. The underlying system, known to experience micro-dynamic effects, can be modelled at a high resolution using one of the proposed approaches. Section 5 concludes the paper.

2 Model and likelihood approximation

In this work we address point-processes with the following, underlying, spatio-temporal autoregressive system

$$\mathbf{x}_{t+1} = \mathbf{A}\mathbf{x}_t + \mathbf{e}_t, \quad (1)$$

where t is a discrete temporal index, each $\mathbf{x}_t \in \mathbb{R}^n$, $\mathbf{e}_t \sim \mathcal{N}(\mathbf{0}, \mathbf{Q}^{-1})$ with both \mathbf{A} and \mathbf{Q} sparse. Equation (1) can be obtained from spatio-temporal models commonly employed in practice, such as the integro-difference equation (IDE) (Wikle, 2002), and the stochastic partial differential equation (SPDE) (Zammit-Mangion et al., 2012b). Sparsity in \mathbf{A} and \mathbf{Q} ensues either by gridding the domain or by employing a Galerkin reduction on an infinite-dimensional system in $z_t(\mathbf{s})$, $\mathbf{s} \in \mathcal{O} \subset \mathbb{R}^2$, using basis functions of compact support. In both cases we can denote the approximate field as $z_t(\mathbf{s}) \approx \boldsymbol{\phi}(\mathbf{s})^T \mathbf{x}_t$ where $\{\boldsymbol{\phi}_i(\mathbf{s})\}_{i=1}^n$ is the basis; when using a grid the approximate field is discontinuous.

As is typical in spatio-temporal point-process applications, we model the intensity function of observed events as $\lambda_t(\mathbf{s}) = \exp(z_t(\mathbf{s}))$; in practice additional covariates may be included, however we omit these in order to facilitate the exposition. Let each observation window be of length Δ_t and $\mathcal{Y}_t = \{\mathbf{s}_i\}_{i \in I_t}$ where I_t is the set of indices corresponding to events in $(t-1, t]$,

then the likelihood of each spatial point process is given by

$$\begin{aligned} p(\mathcal{Y}_t | \mathbf{x}_t) &\propto \exp \left(-\Delta_t \int_{\mathcal{O}} e^{\phi^T(\mathbf{s})\mathbf{x}_t} d\mathbf{s} \right) \prod_{j \in I_t} e^{\phi^T(\mathbf{s}_j)\mathbf{x}_t} \\ &= L_1(\mathbf{x}_t) L_2(\mathbf{x}_t; \mathcal{Y}_t) \end{aligned} \quad (2)$$

This likelihood can be split into two components; the first ($L_1(\mathbf{x}_t)$) is directly related to the *void probability* of the process. We adopt the approach in Simpson et al. (2011) and approximate the integral as:

$$\begin{aligned} \log L_1(\mathbf{x}_t) &\approx -\Delta_t \sum_{i=1}^p \tilde{\eta}_i \exp(\phi^T(\bar{\mathbf{s}}_i)\mathbf{x}_t) \\ &= -\boldsymbol{\eta}^T \exp(\mathbf{C}_1 \mathbf{x}_t), \end{aligned} \quad (3)$$

where $\boldsymbol{\eta} = \Delta_t \tilde{\boldsymbol{\eta}}$ are the scaled integration weights and $\mathbf{C}_1 = [\phi(\bar{\mathbf{s}}_1) \dots \phi(\bar{\mathbf{s}}_p)]^T$ contains the values of the basis at the chosen p integration points $\{\bar{\mathbf{s}}_i\}_{i=1}^p$. The second component of the likelihood, $L_2(\mathbf{x}_t; \mathcal{Y}_t)$, adds contributions from the observed events and can be represented as follows

$$\log L_2(\mathbf{x}_t; \mathcal{Y}_t) = \sum_{j \in I_t} \phi^T(\mathbf{s}_j)\mathbf{x}_t = \mathbf{1}^T \mathbf{C}_2(\mathcal{Y}_t)\mathbf{x}_t, \quad (4)$$

where $\mathbf{C}_2(\mathcal{Y}_t)^T = [\phi(\mathbf{s}_i)]_{i \in I_t}$. The log-likelihood can hence be written, up to a proportionality constant, as

$$\log p(\mathcal{Y}_t | \mathbf{x}_t) \approx -\boldsymbol{\eta}^T \exp(\mathbf{C}_1 \mathbf{x}_t) + \mathbf{1}^T \mathbf{C}_2(\mathcal{Y}_t)\mathbf{x}_t. \quad (5)$$

Both compact basis functions and gridded domains induce sparsity into the observation matrices \mathbf{C}_1 and \mathbf{C}_2 . In particular, if one chooses the integration points to be the vertices of a triangulation or the centres of gridded cells, then \mathbf{C}_1 simplifies to the identity matrix $\mathbf{I}_{n \times n}$ where $n = p$. The integration weights $\tilde{\boldsymbol{\eta}}$ then correspond to the volumes of the basis with unit weight. In addition, $\mathbf{C}_2(\mathcal{Y}_t)$ is again sparse with at most one non-zero element in each row for the gridded case and three non-zero elements per row for the triangulated case.

The spatial discretisation results in a latent Gaussian model. Since \mathbf{C}_1 is the identity and (4) is linear, the non-Gaussian terms will depend on x_{t+1}^j only and from (3) we define the proxy $\psi_{t+1,j}(x_{t+1}^j) = \exp\{-\eta_j \exp(x_{t+1}^j)\}$. Letting $\mathbf{X} = \{\mathbf{x}_t\}_{t=1}^T$ and $\mathcal{Y} = \{\mathcal{Y}_t\}_{t=1}^T$, the latent Gaussian model is given by

$$p(\mathbf{X} | \mathcal{Y}) \propto p_1(\mathbf{x}_1) \prod_t N(\mathbf{x}_{t+1} | \mathbf{A}\mathbf{x}_t, \mathbf{Q}^{-1}) \times \exp(\mathbf{x}_{t+1} \cdot \mathbf{h}_{t+1}^y) \prod_j \psi_{t+1,j}(x_{t+1}^j),$$

where $\mathbf{h}_{t+1}^y = \mathbf{1}^T \mathbf{C}_2(\mathcal{Y}_{t+1})$.

3 Inference

We define the factors¹ $\Psi_{t,t+1}(\mathbf{x}_t, \mathbf{x}_{t+1}) = N(\mathbf{x}_{t+1} | \mathbf{A}\mathbf{x}_t, \mathbf{Q}^{-1}) \exp(\mathbf{x}_{t+1} \cdot \mathbf{h}_{t+1}^y)$ (considering $t = 1$ as a special case) and write

$$p(\mathbf{X} | \mathcal{Y}) \propto \prod_t \Psi_{t,t+1}(\mathbf{x}_t, \mathbf{x}_{t+1}) \prod_j \psi_{t+1,j}(x_{t+1}^j)$$

¹Because of the abundance of indices, we use “.” as a proxy for the inner product.

Note that p can be viewed as a (block) sparse latent Gaussian model and there are various approaches that approximate p and by a (block) Gaussian and apply corrections to it's marginals: (i) the Laplace method and marginal corrections (Rue et al., 2009) (ii) expectation propagation and marginal corrections (Oppel et al., 2009; Cseke and Heskes, 2011) and (iii) the standard variational approximation (no corrections), see (Oppel and Archambeau, 2009). It is generally known that both EP and the variational approach outperform the Laplace method and EP has a computational complexity that scales with that of the Laplace method (Kuss and Rasmussen, 2005; Cseke and Heskes, 2011).

However, since we have a dynamical model, we will try to exploit its structure instead of viewing it as a generic sparse latent Gaussian model. In a similar way as the approach in Heskes et al. (2005), instead of approximating p with a Gaussian q , we only aim to approximate its marginals. We thus define a family of marginals that, as consistency criteria, are assumed to satisfy a set of expectation constraints and define a variational objective to optimise them.

Following standard variational approaches (e.g. Heskes et al., 2005), we use the KL-divergence $D[q||p]$ and its approximations as means to approximate the marginals of p . Due to the factorisation in p we have

$$D[q||p] = - \sum_t E_q[\log \Psi_{t,t+1}] - \sum_{t,j} E_q[\log \psi_{t+1,j}] - H(q) + \log Z_p, \quad (6)$$

where $H(q)$ is the entropy of q and $\log Z_p$ is the (unknown) normalisation constant of p . Note that minimising (6) w.r.t. a q restricted to be Gaussian leads to the standard (block) variational approximation (iii) mentioned above.

To exploit the decomposition of $D[q||p]$ we define a family of approximate marginals $\mathcal{Q} = \{\{q_{t,t+1}^g\}_t, \{q_t^{gs}\}_t, \{q_{t+1,j}^l\}_{t,j}, \{q_{t+1,j}^{ls}\}_{t,j}\}$ which can be viewed as corresponding to the unnormalized density

$$q(\mathbf{X}) \propto \frac{\prod_{t=1}^{T-1} q_{t,t+1}^g(\mathbf{x}_t, \mathbf{x}_{t+1}) \prod_{t=1}^T \prod_j q_{t+1,j}^l(x_{t+1}^j)}{\prod_{t=2}^{T-1} q_t^{gs}(\mathbf{x}_t) \prod_{t=1}^T \prod_j q_{t+1,j}^{ls}(x_{t+1}^j)}. \quad (7)$$

All densities in \mathcal{Q} are approximations of the corresponding marginals and, as we will see later, the optimal marginals lead to a q for which $q(\mathbf{X}) \propto p(\mathbf{X}|\mathcal{Y})$ holds. In particular, $q_{t,t+1}^g$ is assigned to the factor $\Psi_{t,t+1}$ and $q_{t+1,j}^l$ is assigned to $\psi_{t+1,j}$, whereas q_t^{gs} and $q_{t+1,j}^{ls}$ correspond to the separator densities used in graphical models (e.g. Lauritzen, 1996). Let $\mathbf{f}(\mathbf{z})$ be the sufficient statistic of a (sparse) Gaussian with sparsity structure $G(\mathbf{f})$ and let $\mathbf{g}(z) = (z, -z^2/2)$ to denote the sufficient statistic of the univariate Gaussian. We use first and second order statistics as consistency criteria in the approximate marginals, and thus, we define the (temporal) expectation constraints

$$E_{q_{t,t+1}^g}[\mathbf{f}(\mathbf{x}_{t+1})] = E_{q_{t+1}^{gs}}[\mathbf{f}(\mathbf{x}_{t+1})] \quad \text{and} \quad E_{q_{t+1,t+2}^g}[\mathbf{f}(\mathbf{x}_{t+1})] = E_{q_{t+1}^{gs}}[\mathbf{f}(\mathbf{x}_{t+1})]$$

as well as the (spatial) constraints

$$E_{q_{t+1}^l}[\mathbf{g}(x_{t+1}^j)] = E_{q_{t+1}^{ls}}[\mathbf{g}(x_{t+1}^j)] \quad \text{and} \quad E_{q_{t+1}^g}[\mathbf{g}(x_{t+1}^j)] = E_{q_{t+1}^{ls}}[\mathbf{g}(x_{t+1}^j)].$$

When \mathbf{f} corresponds to a fully connected Gaussian, the corresponding temporal expectation constraints are marginal matching constraints. We derive our approach for a general \mathbf{f} and we discuss possible choices in Sections 3.2 and 3.3.

By making use of the tree structure of q , we define the entropy approximation corresponding to \mathcal{Q} by

$$\begin{aligned} -\tilde{H}(\mathcal{Q}) = & \sum_t \mathbb{E}_{q_{t,t+1}^g} [\log q_{t,t+1}^g] - \sum_t \mathbb{E}_{q_t^{gs}} [\log q_t^{gs}] \\ & + \sum_{t,j} [\mathbb{E}_{q_{t+1,j}^l} [\log q_{t+1,j}^l] - \mathbb{E}_{q_{t,j+1}^{ls}} [\log q_{t+1,j}^{ls}]]. \end{aligned}$$

We approximate $\mathbb{E}_q[\log p]$ by using the corresponding members of \mathcal{Q} and arrive to an approximation (without the constant $\log Z_p$) of the variational objective (free energy) in (6) which reads as

$$F(\mathcal{Q}) = - \sum_t \mathbb{E}_{q_{t,t+1}^g} [\log \Psi_{t,t+1}] - \sum_{t,j} \mathbb{E}_{q_{t+1,j}^l} [\log \psi_{t+1,j}] - \tilde{H}(\mathcal{Q}). \quad (8)$$

To deal with the constraints, we introduce the Lagrange multipliers α_{t+1} and β_{t+1} for the (temporal) constraints w.r.t. $q_{t+1,t+2}^g$ and q_{t+1}^{gs} , and $q_{t,t+1}^g$ and q_{t+1}^{gs} , respectively. The multipliers corresponding to the (spatial) constraints on $q_{t,t+1}^g$ and $q_{t+1,j}^{ls}$, and $q_{t+1,j}^l$ and $q_{t+1,j}^{ls}$ will be denoted by $\lambda_{t+1,j}^g$ and $\lambda_{t+1,j}^l$, respectively. The stationary conditions of the Lagrangian corresponding to $F(\mathcal{Q})$ in (8) and the expectation constraints result in the densities

$$\begin{aligned} q_{t,t+1}^g(\mathbf{x}_t, \mathbf{x}_{t+1}) \propto & \Psi_{t,t+1}(\mathbf{x}_t, \mathbf{x}_{t+1}) \exp\left\{\sum_j \lambda_{t+1,j}^g \cdot \mathbf{g}(x_{t+1}^j)\right\} \\ & \times \exp\{\alpha_t \cdot \mathbf{f}(\mathbf{x}_t) + \beta_{t+1} \cdot \mathbf{f}(\mathbf{x}_{t+1})\}, \end{aligned} \quad (9)$$

$$q_{t+1}^{gs}(\mathbf{x}_{t+1}) \propto \exp\{(\alpha_{t+1} + \beta_{t+1}) \cdot \mathbf{f}(\mathbf{x}_{t+1})\}, \quad (10)$$

$$q_{t+1,j}^l(x_{t+1}^j) \propto \psi_{t+1,j}(x_{t+1}^j) \exp\{\lambda_{t+1,j}^l \cdot \mathbf{g}(x_{t+1}^j)\}, \quad (11)$$

$$q_{t+1,j}^{ls}(x_{t+1}^j) \propto \exp\{(\lambda_{t+1,j}^g + \lambda_{t+1,j}^l) \cdot \mathbf{g}(x_{t+1}^j)\}, \quad (12)$$

while the expectation constraints (moment matching) can be rewritten in terms of natural parameters as

$$\text{Collapse}[q_{t,t+1}^g(\mathbf{x}_{t+1}); \mathbf{f}] = \alpha_{t+1} + \beta_{t+1}, \quad (13)$$

$$\text{Collapse}[q_{t+1,t+2}^g(\mathbf{x}_{t+1}); \mathbf{f}] = \alpha_{t+1} + \beta_{t+1}, \quad (14)$$

$$\text{Collapse}[q_{t,t+1}^g(x_{t+1}^j); \mathbf{g}] = \lambda_{t+1,j}^g + \lambda_{t+1,j}^l, \quad (15)$$

$$\text{Collapse}[q_{t+1,j}^l(x_{t+1}^j); \mathbf{g}] = \lambda_{t+1,j}^g + \lambda_{t+1,j}^l. \quad (16)$$

Here, $\text{Collapse}[q; \mathbf{f}]$ and $\text{Collapse}[q; \mathbf{g}]$ are the projections of q into the Gaussian families defined by \mathbf{f} and \mathbf{g} respectively. In other words, let $S(\hat{\mathbf{Q}})$ is the sparsity structure of the matrix $\hat{\mathbf{Q}}$, then

$$\text{Collapse}[q; \mathbf{f}] \equiv \underset{(\hat{\mathbf{h}}, \hat{\mathbf{Q}}): S(\hat{\mathbf{Q}})=G(\mathbf{f})}{\text{argmin}} \quad \mathbb{D}[q || N(\cdot; \hat{\mathbf{Q}}^{-1} \hat{\mathbf{h}}, \hat{\mathbf{Q}}^{-1})].$$

By turning (13) and (14) into a pair of update formulae, we arrive at the well-known forward-backward messages: α_t is the parameter of the forward message and β_{t+1} is the parameter of the backward message. In a similar fashion, the messages corresponding to (15) and (16) correspond to the messages of an expectation propagation algorithm in a latent Gaussian model: $\lambda_{t+1,j}^g$ corresponds to the parameters of the term approximation while $\lambda_{t+1,j}^l$ corresponds to the parameters of the so-called cavity distribution. As a result, the message passing algorithm can be written as

$$\alpha_{t+1}^{new} = \text{Collapse}[q_{t,t+1}^g(\mathbf{x}_{t+1}); \mathbf{f}] - \beta_{t+1}, \quad (17)$$

$$\beta_t^{new} = \text{Collapse}[q_{t,t+1}^g(\mathbf{x}_t); \mathbf{f}] - \alpha_t, \quad (18)$$

$$[\lambda_{t+1,j}^l]^{new} = \text{Collapse}[q_{t,t+1}^g(x_{t+1}^j); \mathbf{g}] - \lambda_{t+1,j}^g, \quad (19)$$

$$[\lambda_{t+1,j}^g]^{new} = \text{Collapse}[q_{t+1,j}^l(x_{t+1}^j); \mathbf{g}] - \lambda_{t+1,j}^l. \quad (20)$$

Appropriate damping of the form $x^{new} = (1 - \epsilon)x^{old} + \epsilon x^{new}$ might need to be applied to help convergence (Heskes et al., 2005). We update $\lambda_{t+1,j}^g$ and $\lambda_{t+1,j}^l$ for all j simultaneously as in Cseke and Heskes (2011).

The message passing updates from above combine both temporal and spatial inference methods in a simple way. They are suited to distributed computations and, as we show in the next section, are more suited to exploit the sparsity of \mathbf{A} and \mathbf{Q} than the typical filtering-smoothing methods that do inference using prediction (marginalisation) and update steps, resulting in operations on full matrices.

3.1 Messages and collapse operations

As can be seen from (17)-(20), the sufficient statistics (structures) of the messages are defined by the expectation constraints, that is, by the Gaussian families defined by \mathbf{f} and \mathbf{g} . In the following we present the details of collapse steps in these equations.

The $\text{Collapse}[q_{t+1,j}^l(x_{t+1}^j); \mathbf{g}]$ step in (20) can be performed as follows. Since $\psi_{t+1,j}$ depends only on x_{t+1}^j , we have to compute the first and second moments of z , where z is distributed according to the un-normalised distribution $\psi_{t+1,j}(z) \exp(hz - qz^2/2)$ and h and q are the corresponding canonical parameters in $\lambda_{t+1,j}^l$. Since this operation cannot be carried out analytically one can resort to numerical approximations by (i) using a change of variables and applying Gauss-Hermite numerical quadrature w.r.t. z or (ii) finding the Gaussian approximation of $\psi_{t+1,j}(z) \exp(hz - qz^2/2)$ by the univariate Laplace method and performing Gauss-Hermite numerical quadrature w.r.t. this approximation. Method (ii) is more accurate when the masses of $\psi_{t+1,j}(z)$ and $\exp(hz - qz^2/2)$ are far apart and is needed mainly in the first few updates; however, because of its better accuracy, we used it throughout the whole procedure. It is applicable in all cases when $\psi_{t+1,j}(z) \exp(hz - qz^2/2)$ is log-concave.

The $\text{Collapse}[q_{t,t+1}^g(\mathbf{x}_{t+1}); \mathbf{g}]$ step in (19) reduces to the computation of the marginal means and variances of $q_{t,t+1}^g(\mathbf{x}_{t+1})$; however, the crucial step is that, in order to preserve sparsity, we carry out the computations on the joint $q_{t,t+1}^g(\mathbf{x}_t, \mathbf{x}_{t+1})$. Let $\alpha_t = (\mathbf{h}_{\alpha_t}, \mathbf{Q}_{\alpha_t})$, $\beta_{t+1} = (\mathbf{h}_{\beta_{t+1}}, \mathbf{Q}_{\beta_{t+1}})$ and $\lambda_{t+1,\cdot}^g = (\mathbf{h}_{\lambda_{t+1,\cdot}^g}, \mathbf{Q}_{\lambda_{t+1,\cdot}^g})$ where $\mathbf{Q}_{\lambda_{t+1,\cdot}^g}$ is diagonal. The precision matrix of $q_{t,t+1}^g$ has the form

$$\mathbf{Q}_t^g = \begin{bmatrix} \mathbf{A}^T \mathbf{Q} \mathbf{A} + \mathbf{Q}_{\alpha_t} & -\mathbf{A}^T \mathbf{Q} \\ -\mathbf{Q} \mathbf{A} & \mathbf{Q} + \mathbf{Q}_{\beta_{t+1}} + \mathbf{Q}_{\lambda_{t+1,\cdot}^g} \end{bmatrix}, \quad (21)$$

where \mathbf{Q}_{α_t} , $\mathbf{Q}_{\beta_{t+1}}$ and $\mathbf{Q}_{\lambda_{t+1}^g}$ are the precision terms corresponding to the messages α_t , β_{t+1} and λ_{t+1}^g . Our task is to (i) solve the system $[\mathbf{Q}_t^g]^{-1}[\mathbf{h}_t^g]$, where $\mathbf{h}_t^{g^T} = [\mathbf{h}_{\alpha_t}^T, \mathbf{h}_{\beta_{t+1}}^T + \mathbf{h}_{t+1}^{g^T} + \mathbf{h}_{\lambda_{t+1}^g}^T]$ and (ii) compute the diagonal of $[\mathbf{Q}_t^g]^{-1}$. A straightforward way is to do a sparse Cholesky factorisation of a convenient reordering of \mathbf{Q}_t^g followed by (i) solving the linear system and (ii) doing a partial inversion by solving the Takahashi equations (Takahashi et al., 1973). Let $\mathbf{L}\mathbf{L}^T = [\mathbf{Q}_t^g]_{\sigma,\sigma}$ where σ is the permutation corresponding to a reordering. Then the partial inversion using the Takahashi equations computes all entries of $[[\mathbf{Q}_t^g]_{\sigma,\sigma}]^{-1}$ for which \mathbf{L} is non-zero. This implies that all entries of $[\mathbf{Q}_t^g]^{-1}$ where \mathbf{Q}_t^g is non-zero are computed (Davis, 2006)—a property which will be further exploited in the Collapse $[\cdot; \mathbf{f}]$ step. The computational complexity of the Takahashi equations scales as $\sum_i (\sum_j S(\mathbf{L})_{ij})^2$ where $S(\mathbf{L})$ is the structure of \mathbf{L} .

The Collapse $[q_{t,t+1}^g(\mathbf{x}_{t+1}); \mathbf{f}]$ and Collapse $[q_{t,t+1}^g(\mathbf{x}_t); \mathbf{f}]$ steps in (17) and (18) can be performed as follows. Let $q(\mathbf{x}) = N(\mathbf{x}|\mathbf{m}, \mathbf{V})$, then Collapse $[q(\mathbf{x}); \mathbf{f}]$ can be expressed as

$$\begin{aligned} & \underset{\hat{\mathbf{Q}}}{\text{minimise}} && \text{tr}(\mathbf{V}\hat{\mathbf{Q}}) - \log \det \hat{\mathbf{Q}} \\ & \text{s.t.} && \hat{\mathbf{Q}}_{i,j} = 0, \text{ for all } (i,j) \notin G(\mathbf{f}), \end{aligned}$$

and compute $\hat{\mathbf{h}} = \hat{\mathbf{Q}}^{-1}\mathbf{m}$. The optimisation can be solved by gradient based methods or the Newton method, however, when the graph $G(\mathbf{f})$ is chordal, optimality conditions lead to equations that can be solved exactly (instead of expensive optimisation) by using the values \mathbf{V}_{ij} with $(i,j) \in G(\mathbf{f})$ (Dahl et al., 2008). Since the covariance values corresponding to the non-zeros in \mathbf{Q}_{α_t} and $\mathbf{Q}_{\beta_{t+1}}$ are all computed when finding the diagonal of $[\mathbf{Q}_t^g]^{-1}$ no further covariance computations are needed thus leading significant computational advantages. For chordal graphs the equations for the optimality conditions can be solved as follows (Dahl et al., 2008). Let C_1, \dots, C_K be the cliques of $G(\mathbf{f})$. Assume further that the cliques of the graph’s junction tree are ordered such that if C_i is an ancestor of C_j then $i \leq j$. Let $S_j = C_j \cap (C_1 \cup C_2 \cup \dots \cup C_{j-1})$ and $R_j = C_j \setminus (C_1 \cup C_2 \cup \dots \cup C_{j-1})$. Then $\hat{\mathbf{Q}} = (\mathbf{I} + \mathbf{U})\mathbf{D}(\mathbf{I} + \mathbf{U})^T$, where \mathbf{U} and \mathbf{D} can be computed iteratively from

$$\mathbf{U}_{R_k, S_k} = -\mathbf{V}_{S_k, S_k}^{-1} \mathbf{V}_{S_k, R_k}, \quad (22)$$

$$\mathbf{D}_{R_k, R_k} = [\mathbf{V}_{R_k, R_k} - \mathbf{V}_{R_k, S_k} \mathbf{V}_{S_k, S_k}^{-1} \mathbf{V}_{S_k, R_k}]^{-1}. \quad (23)$$

The computational complexity scales with $\sum_k \max\{|S_k|^3, |R_k|^3, |S_k|^2|R_k|\}$. The size of the cliques depends on the structure of $G(\mathbf{f})$, see Section 3.3 for further details.

3.2 Inference schemes and scheduling options

The computational complexity is typically dominated by the partial inversion of \mathbf{Q}_t^g . In following we evaluate how different choices of $G(\mathbf{f})$ and message-scheduling strategies influence the number of these operations.

$G(\mathbf{f})$ is fully connected (full). The case of using “full” Gaussian messages can be viewed as comprising the two standard inference schemes: (i) the sequential one, where local message passing is ran till convergence, followed by the passing of temporal messages (this is performed in a cyclic forward backward fashion) and (ii) the static one, where one views the inference as inference on a (block) latent Gaussian field. The latter case corresponds to a

banded partial inversion (Knorr-Held and Rue, 2002) by temporal messages, followed by message exchanges with all $q_{t+1,j}^l$ simultaneously. However, the practical approach to the block model is to use partial matrix inversion (Cseke and Heskes, 2011), instead of banded inversion. As a consequence, **full**, the sequential filtering-smoothing and (block) EP approaches can be viewed as different inference strategies that lead to the same marginal means and variances. Since $G(\mathbf{f})$ is fully connected, we use marginalisation of \mathbf{Q}_t^g by performing Cholesky factorisations (full matrices) on its diagonal sub-blocks. Both $\text{Collapse}[q_{t,t+1}^g(\mathbf{x}_{t+1}); \mathbf{f}]$ and $\text{Collapse}[q_{t,t+1}^g(\mathbf{x}_{t+1}); \mathbf{g}]$ scale as $O(n^3)$.

$G(\mathbf{f})$ is disconnected (diag). This case corresponds to the inference scheme where the temporal messages are factorised. When $G(\mathbf{f})$ is disconnected, \mathbf{Q}_{α_t} and $\mathbf{Q}_{\beta_{t+1}}$ are diagonal, therefore, $\text{Collapse}[:, \mathbf{f}]$ simplifies the corresponding $\text{Collapse}[:, \mathbf{g}]$ -s. The sequential schedule is similar to the **full** scheme, i.e., in each forward or backward step the messages between $q_{t,t+1}^g$ and $q_{t+1,j}^l$ are exchanged until convergence.

$G(\mathbf{f})$ is partially connected (chordal, tsp). The **chordal** case is computationally less intensive than the **full** case both due to the lower connectivity in \mathbf{Q}_{α_t} and $\mathbf{Q}_{\beta_{t+1}}$ (see (21)) and the simpler collapse operations corresponding to (22) and (23). A special case, when $\text{Collapse}(\cdot; \mathbf{f})$ is $O(n)$, is when we choose $G(\mathbf{f})$ as the maximum weight spanning tree of $|\mathbf{A}|$ —we call this **tsp**.

Ideally, we would like to design a message-passing algorithm which achieves convergence with a minimal number of partial inversions steps. Clearly, this is not a straightforward problem to solve. For this reason, we propose a greedy dynamic scheduling where at every step we select the message that has the largest (last) update, and update both the receiver and the source of this message. This is implemented by (i) keeping track of the updates in each $\alpha_t, \beta_t, \lambda_{t+1,j}^g$ and $\lambda_{t+1,j}^l$ and (ii) updating all the outgoing messages when updating an approximate marginal. By constructing longer scheduling queues (ranking the updates) one can distribute the computation to several processing units and achieve a further reduction of computational time.

3.3 Chordal $G(\mathbf{f})$ s and orderings

As shown in Section 3.1, the choice of $G(\mathbf{f})$ and the reordering of \mathbf{Q}_t^g are critical for the good performance of the inference algorithm. Choosing the structure of \mathbf{f} depends on the application or mesh at hand and computational considerations should be taken into account. A reasonable generic choice is the grid or interaction structure. For this reason, we use the structure of \mathbf{A} and we complete it to a chordal graph by adding the least possible number of additional connections, called “fill-in”-s (Davis, 2006). Let $S(\mathbf{A})$ be the sparsity structure of \mathbf{A} . We use its (symbolic) Cholesky factor to complete it to a chordal graph, i.e., for a reordering σ and $S(\mathbf{A}_{\sigma,\sigma}) = S(\mathbf{L})S(\mathbf{L}^T)$, we use $G(\mathbf{f}) = [S(\mathbf{L}) + S(\mathbf{L}^T)]_{\sigma^{-1}, \sigma^{-1}}$. Clearly, some of the additional expectations constraints might not be really meaningful for the model, but they serve to minimise the number of non-zeros in $G(\mathbf{f})$ and thus to reduce the computational costs. We use the following fill-in reducing reorderings: (i) no reordering (**none**, our default node numbering), (ii) the approximate minimum degree (**amd**) permutation, (iii) the symmetric reverse Cuthill-McKee (**rcm**) permutation, and (iv) the nested dissection (**nd**) permutation.

When performing the Cholesky factorisation and partial matrix inversion of \mathbf{Q}_t^g , we consider the same permutation algorithms. We do an empirical estimation of the computational complexity of the $\text{Collapse}[q_{t,t+1}^g; \mathbf{g}]$ and $\text{Collapse}[q_{t,t+1}^g; \mathbf{f}]$ steps and we choose the best per-

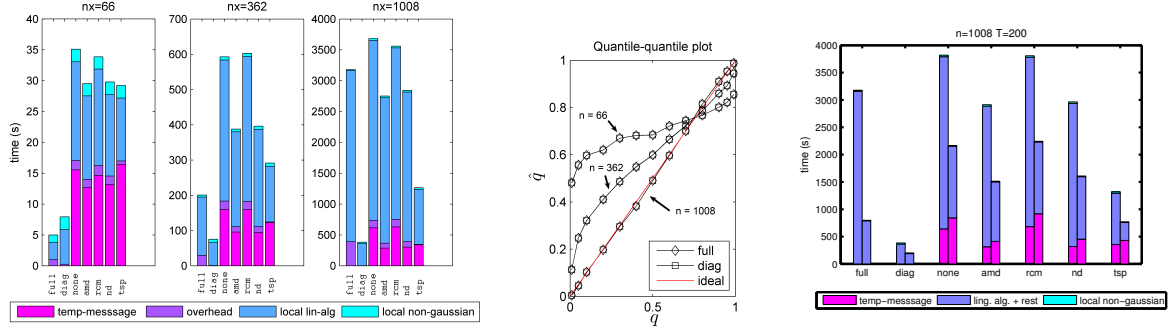


Figure 1: Running times for various state space sizes and scheduling options. (left) Running times for the inference schemes **full**, **diag**, and chordal schemes **none**, **amd**, **rcm**, **nd** and **tsp**. (centre) Quantile-quantile plots for **full** and **diag** with $n = 66, 362, 1008$ in increasing order of accuracy. (right) Comparison in running times of the sequential (left bar) and greedy (right bar) scheduling strategies. Local operations refer for the local EP computations whilst the temporal messages refer to the max-determinant optimisation.

forming pair of permutations. In the models we considered the best performing pairs were the **amd** and **nd** permutations to obtain $G(\mathbf{f})$ —from \mathbf{A} —and **amd** for the factorisation and partial inversion of \mathbf{Q}_t^g . The latter operation typically dominated the computational time and **amd** outperformed the other methods. **amd** and **nd** led to structures in $G(\mathbf{f})$ that resulted in similar computational times (clique size distribution) in the $\text{Collapse}[q_{t,t+1}^g; \mathbf{f}]$ step.

If none of the above mentioned or any other chordal completion strategies are satisfactory, one can revert to a different $G(\mathbf{f})$ and perform the $\text{Collapse}[q_{t,t+1}^g; \mathbf{f}]$ as most appropriate in his/her model’s context (see Section 5).

4 Experiments

In this section we assess the running times and accuracy of the inference methods we introduced and show the potential use of this approach through the **diag** method in the WikiLeaks Afghan War Diary data studied in Zammit-Mangion et al. (2012a). The algorithms were coded in Matlab and we used the partial matrix inversion algorithm of Gerven et al. (2012) which is implemented in C.

4.1 Accuracy

To assess the accuracy of the different methods we constructed a 1-D grid toy model with $n = T = 64$, where at each time point the hidden state at a grid point becomes an average of itself and its 5 neighbours on either side. Hence the matrix \mathbf{A} is banded with bandwidth 5. Each \mathbf{e}_k was sampled with an exponentiated squared covariance with variance 1 and length scale of 5 units (neighbours) - this describes a correlation which decreases from 1 to 0.1 in 3.4 spatial units. The algorithms were assumed to have converged when the maximum absolute change in canonical parameters became less than 10^{-4} .

We generated 150 realisations of this model and assessed the quality using two criteria,

	full	diag	chordal	tsp
$\Delta MTSE$	0	0.018	0.000	0.017
Δq^{bias}	0	3×10^{-4}	3×10^{-6}	3×10^{-4}

Table 1: Algorithmic performance with **full** as reference

(i) the mean total square error per time frame (MTSE) defined as

$$MTSE = \frac{1}{T} \sum_{t=1}^T \sum_{j=1}^n (x_t^{j*} - \hat{x}_t^j)^2$$

where \mathbf{x}_t^* is the simulated realisation and $\hat{\mathbf{x}}_t$ is the marginal mean at time t , and (ii) the quantile-quantile bias, defined as

$$bias_q = q - \frac{1}{Tn} \sum_{t=1}^T \sum_{j=1}^n \mathbf{1}[x_t^{j*} \leq x_t^{jq}]$$

where $\mathbf{1}[\cdot]$ is the indicator function and x_t^{jq} is the inferred threshold of quantile q of the approximate marginal, see Taylor and Diggle (2012) for details. Friedman tests for repeated measures (Field, 2009) found that there were significant differences in both the quantile bias and the MTSEs in the proposed methods ($p < 0.01$). Post-hoc tests showed that **diag** and the **tsp** are, as expected, less accurate than the **chordal** and **full** and that there is no significant difference ($p > 0.2$) between the latter two in both MTSE and bias. The **tsp** only slightly outperformed the **diag**, see Table 1.

Whilst it is hard to generalise conclusions regarding the performance, we do note a slight decrease in performance of **diag** and **tsp** with increasing correlations induced by \mathbf{Q} and \mathbf{A} ; however, in all cases the difference proved to be small relative to the overall performance of the algorithms. It should be noted that in this example a damping $\epsilon = 0.75$ was applied on the temporal messages of **diag** to ensure convergence; because of this it was slower than the **full** and **chordal** schemes. The good performance of the **chordal** is due to the fact that the banded structure is (already) chordal.

4.2 Running times and scalability

To compare running times, we choose a typical scenario where the latent field is governed by

$$\begin{aligned} dz(\mathbf{s}, t) &= \mathcal{A}z(\mathbf{s}, t)dt + dW(\mathbf{s}, t), \\ z(\mathbf{s}, 0) &= z_0(\mathbf{s}), \end{aligned} \tag{24}$$

with $W(\mathbf{s}, t)$ being a space-time Wiener process having a covariance operator $\Sigma u(\mathbf{s}) = \int k(\mathbf{s}, \mathbf{r})u(\mathbf{r})d\mathbf{r}$. The operator $\mathcal{A} = D\Delta(\cdot)$ where $\Delta(\cdot)$ is the Laplacian and we used a circular domain for \mathcal{O} with radius r . Temporal discretisation with $\Delta_t = 0.01$ followed by the Galerkin method in conjunction with a row-sum lumping method (Bueche et al., 2000; Lindgren et al., 2011) was applied to obtain a sparse matrix \mathbf{A} with $n = 2267$ for simulating data with $T = 200$. We set $r = 10$, $D = 0.2$ and assumed that the discretised precision matrix

\mathbf{Q} is diagonal with elements $1/15$.² We found that under this configuration, at stationarity, around 1000 points per time frame were generated; a typical count for large data sets.

The algorithms were tested on Delaunay triangulations of the domain constructed using routines by Persson and Strang (2004) with varying mesh density, $n \in \{362, 562, 1008\}$. Computational times were recorded using Matlab’s profiler. In both the static and sequential scheduling schemes, $\lambda_{t+1,\cdot}^{gs}$ and $\lambda_{t+1,\cdot}^{ls}$ messages were run till convergence. To ensure a fair comparison, all test results given here are with computations restricted to a single processor core.³

The computational times for the sequential scheduling are plotted in the left panel of Figure 1. We segmented the computational times to correspond to the three main collapse operations: (1) *temporal messages* stands for the max determinant optimisation problem (overhead in **full**) (2) *overhead* accounts for initialisations, updating messages and monitoring convergence (3) *lin- alg* logs the time for linear algebraic operations (Cholesky factorisation, partial matrix inversion), and (4) *non-Gaussian* stands for the univariate moment matching. For clarity, we omit results for the static case which was up to an order of magnitude slower than the second worst-performing method. This slow performance is attributed to the number of iterations required for convergence, which is more than the number of forward-backward cycles required by the **full**.

The left panel in Figure 1 shows that, for small n , the **full** inference scheme is faster than the other schemes due to the fact that it is implemented more efficiently in terms of matrix operations. However, the situation changes for large n and for $n = 1008$, where we see that the **full** is slower than the best **chordal** methods and much slower than the **tsp** and **diag**. Note that the increase in computational time is well below cubic and at most quadratic for all methods other than the **full**. We could not run the **full** for larger n due to memory restrictions. As shown in the centre panel of Figure 1, in this case the increased speed does not come at a loss in distributional accuracy and despite the data being simulated at $n = 2267$ quantification of uncertainty at $n = 1008$ is very good for all methods. This was unexpected given the correlations induced by \mathbf{A} ; at this stage it is not yet clear to which extent the performance of the **diag** varies with the parameters of the system.

A small note is due on the speed-ups made possible when using greedy scheduling, as opposed to sequential scheduling (see right panel in Figure 1). Although the scheduling itself does not affect the scalability of the algorithm, it can be seen that, as expected, the greedy scheduling can drastically reduce the computational time. For instance, after the initial forward-backward, the **full** needed only a few factor updates to achieve convergence within tolerance.

4.3 The Afghan War Diary

Zammit-Mangion et al. (2012) introduced point-process modelling methods for conflict and employed an algorithm similar to the **full** described here in an iterative state-parameter update scheme on the WikiLeaks Afghan War Diary (AWD). However modelling of micro-scale effects such as relocation or escalation diffusions in conflict (Schutte and Weidmann, 2011) were not possible at the resolution considered; whilst an average basis there had a scope

²This follows when modelling the covariance function $k(\mathbf{s}, \mathbf{r}) = \sum_i \phi_i(\mathbf{s})\phi_i(\mathbf{r})\tilde{\lambda}_i = \boldsymbol{\phi}(\mathbf{s})^T \mathbf{\Lambda} \boldsymbol{\phi}(\mathbf{r})$.

³All algorithms were tested on an Intel® Core™i7-2600S @ 2.80GHz personal computer with 8GB of RAM.

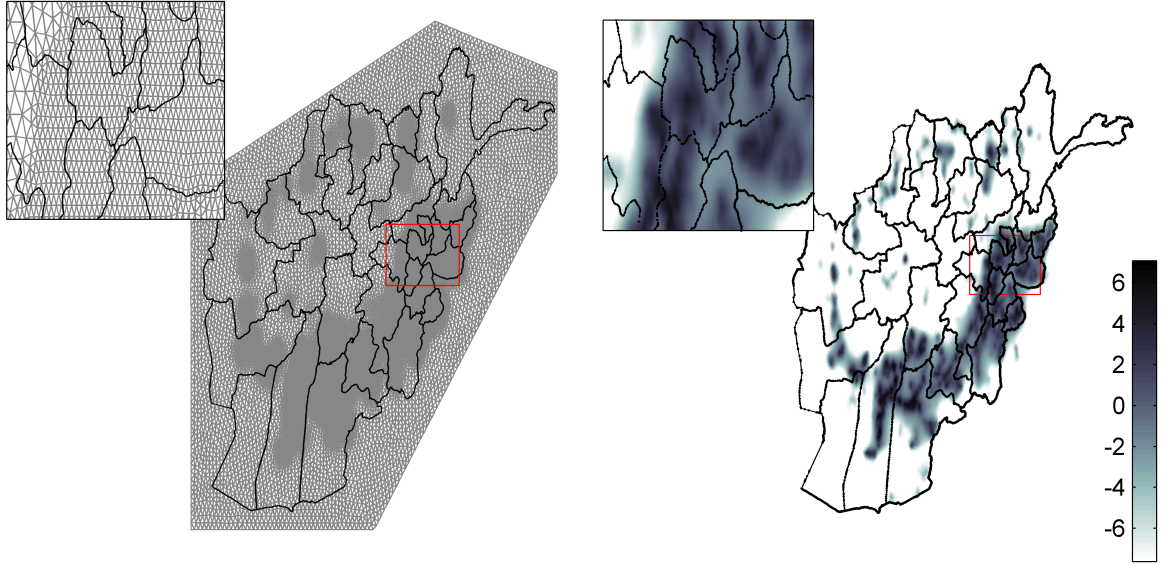


Figure 2: The mesh and one time-slice log intensity map corresponding to the AWD on the first week of October 2009.

on the order of 100km, conflict diffusions are observed at resolutions of ≈ 10 km. The scope here is to show that we can perform inference on the required spatial and temporal scales.

We assembled a mesh on Afghanistan using population density as a proxy for mesh density. The resulting construction, shown in Figure 2 has the largest triangles with sides of 22km and the smallest ones with sides of 7km. The total number of vertices amounts to $n = 9398$ in a system with $T = 313$ time points (weeks). We constructed \mathbf{A} from the diffusion equation above with $D = 1 \times 10^{-4}$ with latitude/longitude used as spatial units. $\sigma_w^2 = 0.2$ was taken as rough value from the full joint analysis using a low resolution model, see Zammit-Mangion et al. (2012a) for details.

We carried out inference in the AWD with the `diag` algorithm. A characteristic plot showing one week of the conflict progression (first week of October 2009) is given in Figure 2. At this point in the conflict activity in the south in Helmand and Kandahar was reaching its peak and conflict at the Pakistani border was intensifying considerably. The insets show how detailed inferences can be made - note that here we have employed fixed hyperparameters; spatially-varying smoothness as in (Lindgren et al., 2011) may be introduced in the model with relative ease. Inference completed in just over 5 hours on a standard PC and consumed only about 4GB of memory. This performance implies that, with appropriate exploitation of clustered/distributed computational resources, full state-parameter inference of very large systems can be carried out in considerably shorter timescales and with potentially less resources than previously envisioned.

5 Conclusions

In this paper we have presented a family of EP inference methods for spatio-temporal log-Gaussian Cox process models; the algorithms are based on approximate inference methods

using expectation constraints. We show how the sparsity in the underlying dynamic model can be exploited in order to overcome the limitations in the standard forward-backward and block inference schemes which can become expensive w.r.t. both storage and computation for large n and T . Our approach is applicable in any similar sparse latent linear dynamical model. For the models we studied, **diag** is faster but less accurate than **chordal**. The inference schemes using messages with chordal precision structures can serve as a compromise in complexity between schemes using diagonal and full precision matrix structures.

In the future we intend to explore the set of structures that lie between the fast and less accurate spanning tree and the somewhat larger chordal structures employed in this work. We are currently working on including parameter inference and correction methods (Cseke and Heskes, 2011) in the methodological framework; this will be addressed in a follow-up paper.

References

- D. Bueche, N. Sukumar, and B. Moran. Dispersive properties of the natural element method. *Computational Mechanics*, 25(2):207–219, 2000.
- B. Cseke and T. Heskes. Approximate marginals in latent Gaussian models. *Journal of Machine Learning Research*, 12:417–454, 2011.
- J. Dahl, L. Vandenberghe, and V. Roychowdhury. Covariance selection for nonchordal graphs via chordal embedding. *Optimization Methods Software*, 23(4):501–520, Aug. 2008.
- T. A. Davis. *Direct Methods for Sparse Linear Systems (Fundamentals of Algorithms 2)*. Society for Industrial and Applied Mathematics, Philadelphia, PA, USA, 2006.
- P. Diggle, B. Rowlingson, and T. Su. Point process methodology for on-line spatio-temporal disease surveillance. *Environmetrics*, 16(5):423–434, 2005.
- A. Field. *Discovering statistics using SPSS*. Sage Publications Limited, 2009.
- M. Gerven, A. Bahramisharif, J. Farquhar, and T. Heskes. Donders machine learning toolbox, 2012. URL <https://github.com/distrep/DMLT>.
- J. Hartikainen, J. Riihimäki, and S. Särkkä. Sparse spatio-temporal Gaussian processes with general likelihoods. In *Proceedings of the 21th International Conference on Artificial Neural Networks - Volume Part I*, ICANN’11, pages 193–200. Springer-Verlag, 2011.
- T. Heskes, M. Opper, W. Wiegierinck, O. Winther, and O. Zoeter. Approximate inference techniques with expectation constraints. *Journal of Statistical Mechanics: Theory and Experiment*, 2005.
- M. B. Hooten and C. K. Wikle. A hierarchical Bayesian non-linear spatio-temporal model for the spread of invasive species with application to the Eurasian Collared-Dove. *Environmental and Ecological Statistics*, 15(1):59–70, Mar. 2008.
- L. Knorr-Held and H. Rue. On block updating in Markov random field models for disease mapping. *Scandinavian Journal of Statistics*, 29(4):597–614, Dec. 2002.
- M. Kuss and C. E. Rasmussen. Assessing approximate inference for binary Gaussian process classification. *Journal of Machine Learning Research*, 6:1679–1704, 2005. ISSN 1533-7928.
- S. L. Lauritzen. *Graphical Models*. Oxford Statistical Science Series. Oxford University Press, New York, USA, July 1996. ISBN 0198522193.

- F. Lindgren, H. Rue, and J. Lindström. An explicit link between Gaussian fields and Gaussian Markov random fields: the stochastic partial differential equation approach. *Journal of the Royal Statistical Society B*, 73(4):423–498, Sep. 2011.
- K. P. Murphy and Y. Weiss. The factored frontier algorithm for approximate inference in dbns. In *Proceedings of the 17th Conference in Uncertainty in Artificial Intelligence*, pages 378–385, 2001.
- M. Opper and C. Archambeau. The variational Gaussian approximation revisited. *Neural Computation*, 21(3):786–792, 2009.
- M. Opper, U. Paquet, and O. Winther. Improving on expectation propagation. In D. Koller, D. Schuurmans, Y. Bengio, and L. Bottou, editors, *Advances in Neural Information Processing Systems 21*, pages 1241–1248. MIT, Cambridge, MA, US, 2009.
- P. Persson and G. Strang. A simple mesh generator in MATLAB. *SIAM review*, pages 329–345, 2004.
- A. Rodrigues and P. J. Diggle. Bayesian estimation and prediction for inhomogeneous spatiotemporal log-Gaussian Cox processes using low-rank models, with application to criminal surveillance. *Journal of the American Statistical Association*, 107(497):93–101, 2012.
- H. Rue, S. Martino, and N. Chopin. Approximate Bayesian inference for latent Gaussian models by using integrated nested Laplace approximations. *Journal Of The Royal Statistical Society B*, 71(2):319–392, 2009.
- S. Schutte and N. B. Weidmann. Diffusion patterns of violence in civil wars. *Political Geography*, 30:143–152, 2011.
- D. Simpson, J. Illian, F. Lindgren, S. Sørbye, and H. Rue. Going off grid: Computationally efficient inference for log-Gaussian Cox processes. *arXiv preprint arXiv:1111.0641*, 2011.
- K. Takahashi, J. Fagan, and M.-S. Chin. Formation of a sparse impedance matrix and its application to short circuit study. In *Proceedings of the 8th PICA Conference*, 1973.
- B. M. Taylor and P. J. Diggle. INLA or MCMC? A tutorial and comparative evaluation for spatial prediction in log-Gaussian Cox processes. *arXiv preprint arXiv:1202.1738v2*, 2012.
- C. K. Wikle. A kernel-based spectral model for non-Gaussian spatio-temporal processes. *Statistical Modelling*, 2(1):299–314, 2002.
- A. Zammit-Mangion, G. Dewar, M., K. V., A., and G. Sanguinetti. Point process modelling of the Afghan war diary. *Proceeding of the National Academy of Sciences*, 2012a. doi: 10.1073/pnas.1203177109.
- A. Zammit-Mangion, G. Sanguinetti, and V. Kadirkamanathan. Variational estimation in spatiotemporal systems from continuous and point-process observations. *IEEE Transactions on Signal Processing*, 60(7):3449–3459, 2012b.